**AIAA 2002-5220**

# Progress in the Design of a Reusable Launch Vehicle Stage

*Martin Sippel, Josef Klevanski, Holger Burkhardt*
*Space Launcher Systems Analysis (SART), DLR, Cologne, Germany*
*Thino Eggers, Ognjan Božić*
*Institute of Aerodynamics and Flow Technology, DLR, Braunschweig, Germany*
*Philipp Langholf*
*MAN-Technologie AG, Augsburg, Germany*
*Andreas Rittweger*
*Astrium GmbH, Bremen, Germany*

**The German future launcher technology research program ASTRA investigates in its system study two types of partially reusable launch vehicles. This paper describes one of those concepts, a reusable first stage designed for a near term application with a heavy lift launcher. The attached reference expendable space transportation system is a future Ariane 5 with cryogenic core and upper stage, but skipped solid rocket boosters. The design of the reference liquid fly-back boosters (LFBB) is focused on LOX/LH2 propellant and a future derivative of the Vulcain rocket motor.**

**After achieving a convergent design in the first iteration loop, a more detailed level of investigation has been started. This includes the ascent control requirements on the booster TVC system, a refinement of the aerodynamic shape, and the preliminary mechanical lay-out of body and wing structure. All major results are presented, and used in an update of the mass budget, as well as trajectory simulations and optimizations for ascent and reentry.**

### Nomenclature

| | | |
|---|---|---|
| D | Drag | N |
| M | Mach-number | - |
| Q | heat flux | $W/m^2$ |
| T | Thrust | N |
| W | weight | N |
| l | body length | m |
| m | mass | kg |
| sfc | specific fuel consumption | g/kNs |
| q | dynamic pressure | Pa |
| v | velocity | m/s |
| $\Pi$ | ratio of total pressures $P_i/P_{i-1}$ | - |
| $\alpha$ | angle of attack | - |
| $\gamma$ | flight path angle | - |
| $\delta$ | deflection angle | - |
| $\varepsilon$ | expansion ratio | - |
| $\eta$ | control surface defection angle | - |
| $\lambda$ | bypass-ratio | - |
| $\vartheta$ | pitch angle | - |
| $\omega_y$ | pitch velocity | $s^{-1}$ |

### Subscripts, Abbreviations

| | |
|---|---|
| AFRSI | Advanced Flexible Reusable Surface Insulation |
| AOA | angle of attack |
| CAD | computer aided design |
| CFRP | Carbon Fiber Reinforced Polymer |
| EAP | Etage d'Accélération à Poudre (of Ariane 5) |
| EPC | Etage Principal Cryotechnique (of Ariane 5) |
| ESC-B | Etage Supérieur Cryotechnique (of Ariane 5) |
| FEM | finite element method |
| GLOW | Gross Lift-Off Mass |
| GTO | Geostationary Transfer Orbit |
| H2K | Hypersonic Wind Tunnel (at DLR Cologne) |
| JAVE | Jupe AVant Equipée (forward skirt of Ariane 5) |
| LFBB | Liquid Fly-Back Booster |
| LH2 | Liquid Hydrogen |
| LOX | Liquid Oxygen |
| MECO | Main Engine Cut Off |
| SRM | Solid Rocket Motor |
| TMK | Trisonic Test Section (at DLR Cologne) |
| TVC | Thrust Vector Control |
| can | canard |
| cog | center of gravity |
| sep | separation |
| s/l | sea-level |
| 0,0 | sea-level, static conditions |
| $x_S$ | x-coordinate of the center of gravity |
| $x_N$ | neutral point position |

## 1 INTRODUCTION

Within the system studies of the German future launcher technology research program ASTRA two reusable first stage designs are under investigation. The one dedicated for near term application with an existing expendable core stage, is called a winged fly-back booster. As one of the results of the ASTRA-analyses of the years 2000 and 2001, it can be stated, that such a reusable booster stage in connection with the unchanged Ariane 5 expendable core stage is technically feasible, and competitive with other reusable and advanced expendable launchers.

The basic design philosophy is to choose a robust vehicle, which gives a relatively high degree of confidence to achieve the promised performance and cost estimations. In the second part of the research study 'lessons learned' from the first phase and previous investigations (e.g. ref. 1 to 3) are integrated. This notably means, find an acceptable solution for the hypersonic and subsonic cruise trim requirements by refining the aerodynamic con-

figuration. A major point is to improve the mechanical lay-out and introduce a structurally based mass estimation to gain a more solid basis for a forthcoming development decision. As far as possible the applicability of existing and already qualified parts should be assessed for integration in the booster stage.

## 2 OVERVIEW OF THE INVESTIGATED SEMI-REUSABLE LAUNCH VEHICLE

The regarded partially reusable space transportation system consists of dual booster stages, which are attached to the expendable Ariane 5 core stage (EPC) at an upgraded future technology level. The EPC stage is assumed to be powered by a single advanced derivative of the Vulcain engine with increased vacuum thrust, and contains about 185000 kg of subcooled propellants. A new cryogenic upper stage (ESC-B) is already in the development phase. It should include a new advanced expander cycle motor of 180 kN class (VINCI) by 2006.

Two symmetrically attached reusable boosters accelerate the expendable Ariane 5 core stage (Figure 1). They should replace the solid rocket motors EAP in use today.

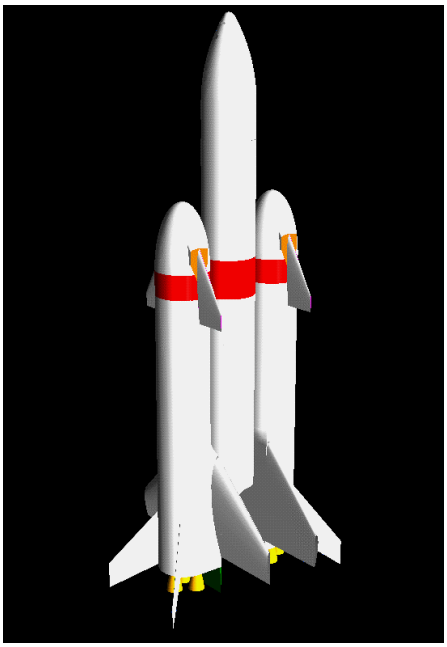

**Figure 1: Semi-reusable launch vehicle with Ariane 5 core stage and two attached reusable fly-back boosters**

### 2.1 LFBB Geometry Data and Lay-Out

The reusable booster stage is based on the same advanced version of the EPC's Vulcain engine, but employs an adapted nozzle with reduced expansion ratio. The engines are installed in a group of three in a circular arrangement in the vehicles back. Overall LFBB length is 42 m. A fuselage and outer tank diameter of 5.45 m is selected, to achieve a high commonality with Ariane's main cryogenic stage EPC.

Three air-breathing engines for fly-back are installed in the vehicle's nose section (see Figure 2), which also houses the RCS and the front landing gear. The nose is of ellipsoidal shape with a length of 6.7 m. The positions of the turbo-engines is selected with regard to integration requirements of the core engine, as well as the exhaust duct. The recent design locates the complete RCS in the nose to provide sufficient torque with regard to vehicle cog.

The nose section is followed by an annular attachment structure, for which a more detailed description is given in chapter 5.2. The structure for canard mounting and actuation is provided at the center of this attachment ring. The following cylindrical tank is integral and of similar lay-out as for the EPC core stage with same diameter but shortened length. This geometry constraint might reduce manufacturing costs if realized, and enables to better compare expendable with reusable structures within this investigation. LOX is stored in the upper position, separated by a common bulkhead from the first LH2 tank. The ascent propellant mass reaches 165000 kg when a subcooling and hence density increase of LOX to 1240 kg/m$^3$ and to 76 kg/m$^3$ for super-cooled LH2 can be achieved. It is assumed to install both the cryo- and thermal insulation externally. This approach is preferred to any arrangement inside, to have better accessibility of the tank walls for inspection between two flights. The integral tank section is followed by the wing and fuselage frame section. A second, non-integral LH2 tank is mounted above the wing carry-through. This tank is interconnected with the main hydrogen tank, and it is currently foreseen to perform the engine feed through this second tank.

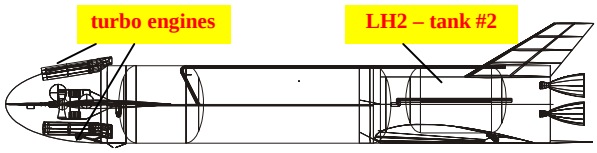


**Figure 2: LFBB projection in the x-z-plane**

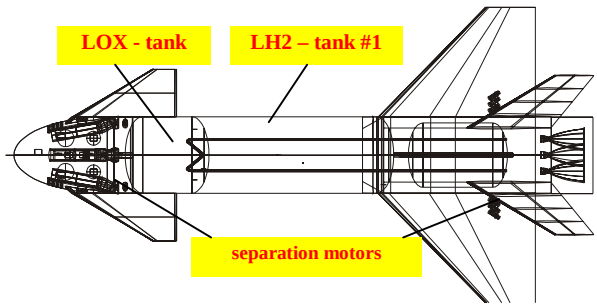


**Figure 3: LFBB projection in the x-y-plane**

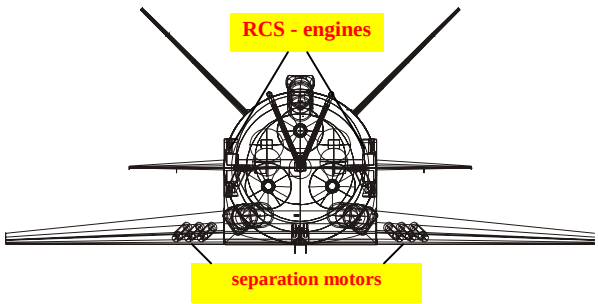


**Figure 4: LFBB projection in the y-z-plane**

The main wing lay-out is presently based on an airfoil with flat lower surface. This type is chosen because the flat lower side is advantageous in hypersonic flow. The complete aerodynamic configuration, including the required deflection angle of the canards, has been preliminarily checked on its trim performance during the

full return flight trajectory. (see chapters 4 and 6) The wing span reaches more than 21 m and the exposed area is about 115 $m^2$.

The rocket engines are mounted on a thrustframe. A full 2D gimballing of all engines is required to obtain sufficient controllability of the launch vehicle (see chapter 3). The engines are protected on the lower side by a body flap, also necessary for aerodynamic trimming and control. Two vertical fins are attached to the upper part of the fuselage, inclined by 45 deg. (see Figure 4). The structural support of the complete launch vehicle on the launch table has to be provided by the two LFBB.

## 2.2 Propulsion System Data

An advanced, more puissant version 2 of the European cryogenic gas-generator cycle rocket engine Vulcain is under development, and will be operational in 2002. An even more powerful Vulcain 3 is currently in definition studies. It might include increased mass flow, higher chamber pressure, and a larger expansion ratio. Although no technical data are fixed yet, the presented results of this paper, and the ASTRA-study is based on assumptions concerning the performance of this motor. Engine data of the advanced Vulcain variant with reduced expansion ratio to be used in the LFBB configuration are given in Table 1.

| Cycle | open gas-generator | |
|---|---|---|
| propellant combination | LOX / LH2 | |
| nominal thrust (s/l) | 1412 | kN |
| nominal thrust (vacuum) | 1622 | kN |
| specific impulse (s/l) | 367.23 | s |
| specific impulse (vacuum) | 421.7 | s |
| chamber pressure | 13.9 | MPa |
| mixture ratio | 5.9 | - |
| nozzle area ratio | 35 | - |
| length | 2890 | mm |
| diameter | 1625 | mm |
| dry weight | 2370 | kg |
| T/W (s/l) | 60.7 | - |
| T/W (vacuum) | 69.8 | - |

**Table 1: Proposed Vulcain 3 (ε= 35) main engine characteristics as used in the study**

To reduce the mass of fly-back fuel, turbo engines which use hydrogen should be implemented. The replacement of kerosene by hydrogen is not an insurmountable problem, although the special requirements for the existing military turbofan EJ-200 will be addressed within the ASTRA-study. The engines will be installed without afterburner and have a nozzle with fixed throat. Mach and altitude dependent data sets are calculated regarding the Kourou atmospheric conditions. Main technical data at sea-level are given in Table 2.

The reaction control system (RCS) thrust requirements are defined with regard to the only flown RLVs: The Space Shuttle and the Buran orbiter. The sizing of the Space Shuttle RCS thrusters is based on the yaw acceleration for re-entry attitude control. At maximum vehicle mass about 0.5 °/$s^2$ has to be achieved [5]. Buran had obviously been designed in an analogous manner. In case of the LFBB configuration these requirement leads to 10 thrusters on each side of the vehicle with a thrust level of 2 kN per engine. Currently different propellant combinations are looked upon. Besides the classical but toxic $N_2O_4$ / MMH, the environmentally friendly $GO_2$ / Ethanol and $GO_2$ / $GH_2$ are regarded. The latter have an operational advantage for a reusable system, but need to be proven concerning reliable ignition capability under all circumstances. Cryogenics have been disregarded due to concern about freezing of feed lines or valves. The low density $GH_2$ needs a large and heavy tank, which nevertheless can be integrated in the nose section. Preliminary RCS dimensioning is done by Astrium with some heritage in testing of advanced propellants for this type of engines. [6]

| OPR | - | 26 |
|---|---|---|
| $\Pi_{FAN/LPC}$ | - | 4.35 (3 Stages) |
| $\Pi_{HPC}$ | - | 5.98 (5 Stages) |
| HP-Turbine | - | 1 Stage |
| LP-Turbine | - | 1 Stage |
| Bypass ratio λ | - | 0.4 |
| air mass flow | kg/s | 77 |
| TET | K | 1800 |
| $F_{0,0}$ , dry | N | 54000 |
| $sfc_{0,0}$ , dry | g/kNs | 8.1 |

**Table 2: EJ-200 technical specification data at Kourou sea-level static conditions and hydrogen propellant according to *abp* [4] calculation**

The last propulsion system of the LFBB are the solid separation motors, which provide a safe separation after booster MECO. Two of them are located in the attachment ring, and further six are integrated symmetrically on the lower side of the wing. (see Figure 3 and Figure 4) The motor design is similar to that of today's Ariane 5 separation system, but with increased propellant loading. The additional amount is required because of the increased separation mass of the reusable stage compared to the expendable SRM.

# 3 ASCENT CONTROL

A launcher with a dual winged booster configuration is subject to increased wind and gust perturbations compared with a fully expendable system without wings. Therefore, the controllability during ascent flight is to be verified. In a dynamic simulation, control is performed by thrust vector gimballing of all available rocket engines of the two boosters. A simple 2D flight mechanical model is used throughout the investigation of ascent controllability. Conservative assumptions for boundary conditions are taken, to obtain results with high confidence.

The launcher configuration's orientation in the nominal case pitches versa the east with the main wings perpendicular to the flow. This configuration is however quite insensitive to the more powerful east-west wind. It is therefore necessary in the 2-D study to turn the launch vehicle by 90° to estimate appropriately the controllability during ascent flight for a worst case scenario of wind loads.

## 3.1 Mass and Inertia Model

The launcher is modeled using simple geometrical structures to calculate mass and moments of inertia. The

propellant center of mass can be rapidly calculated for different filling levels assuming cylindrical tanks. The moments of inertia are obtained using the formula for cylindrical solids, neglecting fluid dynamic effects.

The center of gravity evolves during ascent flight due to the consumption of propellant. A linear interpolation between the initial and final value is chosen for the propellant mass of each tank separately, which is a good approximation in the case of cylindrical tanks and constant mass flow. The total pitching moment of inertia is completely calculated with regard to the launcher center of gravity position at each instant of the trajectory. The inertia of the propellants is linearly interpolated in each tank likewise as the cog movement.

### 3.2 Aerodynamic Model

The ascent control analysis requires complete data sets of the aerodynamic coefficients $C_D$ (Drag), $C_L$ (Lift) and $C_M$ (Momentum) as function of the angle of attack and Mach number for the complete ascent configuration. These sets can not be obtained by sophisticated calculations in this early phase of preliminary design. Theoretical and empirical methods are used to calculate data for fuselages, wings and wing sections. Aerodynamic coefficients for the whole launcher are then obtained by linear superposition. The quality of the implied method for pre-analysis studies has been demonstrated for various launcher and hypersonic configurations [7].

Interference forces are not considered in this simple, but fast and efficient approach. Note, that this is a conservative assumption for the regarded launcher configuration. This is especially true at high angle of attack flight, due to actual partial shading of the second wing and body not considered in this aerodynamic force calculation.

### 3.3 Wind Model

Wind is modeled according to GRAM-95 (see Figure 5). In accordance to 2D flight dynamics, the mean east-west wind for Jan 01 2010 (high solar activity) is simulated.

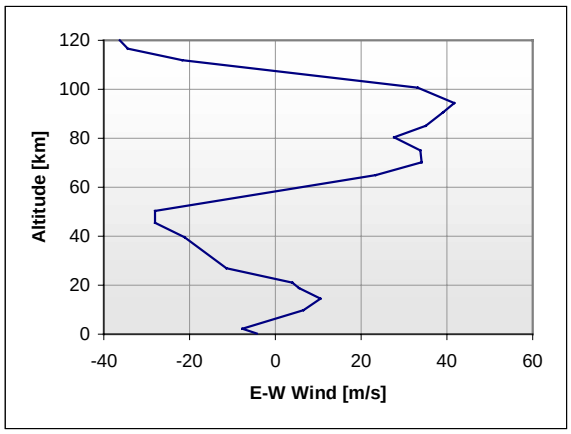


**Figure 5: Mean wind in east-west course at Kourou, projection for 2010**

Additionally, an instantaneous, angle of attack augmenting gust of 10 m/s is applied during the ascent flight simulations. The time of the gusts after lift-off is parametrically varied.

### 3.4 Flight dynamic Model and Control System

The simulation is done with a simplified flight dynamic model. Flight in 2D over flat earth is assumed. The differential equations are integrated numerically with a fixed time step of 0.01 s. The closed loop control system follows the optimal ascent flight trajectory already calculated in a 3DOF optimization. The external disturbances as e.g. wind have to be compensated. The principal control algorithm complies with the following law and its control system coefficients k:

$$\delta_{TVC} = k_{\omega_y} \cdot \omega_y + k_{\vartheta} \cdot \int (\vartheta_{set} - \vartheta_{act}) dt$$

All six booster engines are used for control purposes in the nominal case. The nozzle actuators are modeled as a proportional element with a threshold of 0.1°. The maximum deflection of the nozzles is limited to 5.5°, maximum gimbal velocity is limited to 10°/s. These values are well within the operational constraints of the current Ariane 5 EPC.

### 3.5 Results of dynamic ascent calculation

In a systematical approach, various winged LFBB launcher configurations with Ariane 5 had been analyzed on their sensitivity to atmospheric perturbations [8]. The simulations show that the nominal vehicle without gusts perpendicular to the wings is insensitive to changing wind conditions. The maximum nozzle deflection during the ascent flight stays below 1°. This result is in coherence with expectations as the cross section opposed to wind forces is only merely bigger than for a standard Ariane 5 configuration.

The most critical instant during the ascent flight is identified at about 30 s after lift-off. The maximal obtained deflection of the booster engines takes an extreme value for a wind gust at that time [8]. This outcome is in coherence with expectations based on the evolution of the product of angle of attack times dynamic pressure $(q \cdot \alpha)_{max}$. Another result of this analysis is that both, a reduced wing size and a forward position reduce the control effort and augment margins.

The following figures show plots of characteristic parameters during the ascent flight, where it is assumed that the whole wing surface is exposed to the wind and the aerodynamic moments are therefore bigger. A gust of 10 m/s is introduced at 30 s. The transverse $n_z$ and axial load factors $n_x$ are depicted in Figure 6. The impact of the atmospheric perturbation can clearly be seen, even though $n_z$ never exceeds 0.3 g.

The angular pitch velocity (Figure 7) reaches a peak of slightly below -1.2 degrees /s immediately after the gust. The other pitching movement is the result of the changing wind profile and the requirement to follow pitch angle of the optimized ascent trajectory.

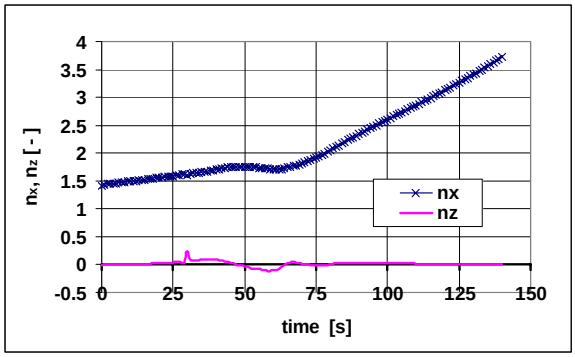


**Figure 6: Load factors $n_x$ and $n_z$ as function of ascent flight time for an LFBB configuration subject to wind and gust**

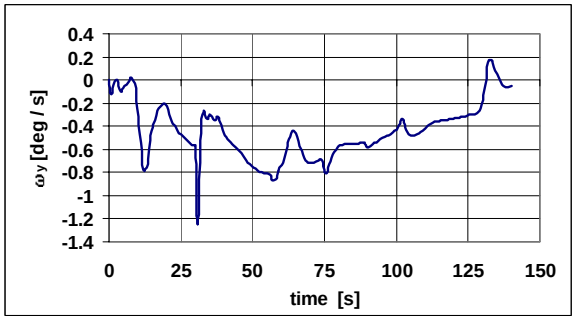


**Figure 7: Angular pitch velocity $\omega_y$ as function of ascent flight time for an LFBB configuration subject to wind and gust**

The required nozzle deflection angle of all six booster engines to counter the perturbation is shown in Figure 8. The simulation shows that the most demanding deflection value of approximately –3 degrees stays well below the limits of 5.5°. The remaining maneuvering margin is however reduced. The presented results as well as previous studies [8] proof the controllability of the examined launcher configurations during the mated ascent until booster separation, if all booster engines are available for two dimensional thrust vector control. The study indicates that the ascent flight requirements of control seem to be *not* the dimensioning factor for wing layout and positioning.

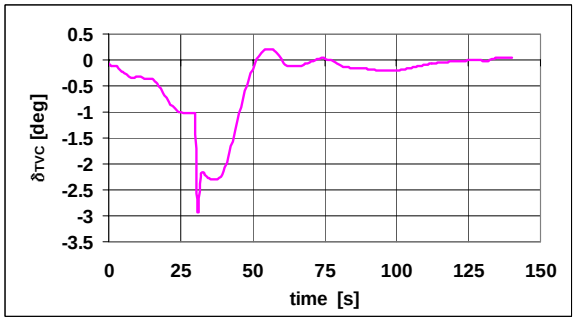


**Figure 8: Thrust vector deflection angle $\delta_{TVC}$ as function of ascent flight time for an LFBB configuration subject to wind and gust**

## 4 AERODYNAMIC DESIGN AND ANALYSIS

The applied aerodynamic and flight dynamic simulation of the return flight requires trimmed aerodynamic data sets for the complete trajectory from separation at M=7 down to the landing phase at M=0.27. The resulting configuration has to comply with tight margins concerning longitudinal stability and trim and the behaviour of the booster has to be robust over the complete Mach number range. Another demand is the analysis of the transonic flight regime. These boundary conditions require the application of aerodynamic codes which allow to resolve even small geometric effects.

Therefore, the aerodynamic work is based on unstructured Euler simulations for M < 2 (DLR TAU code [9]) and surface inclination methods are used for M > 2 (DLR HOTSOSE code [10]). One goal of the study is to provide a complete aerodynamic data set for trim and balance. Additionally, the obtained results are the basis for the definition of a wind tunnel model (Figure 9) to be investigated in the DLR wind tunnels TMK and H2K. The force measurements at Mach numbers between 0.5 < M < 7 are planned for the end of 2002. They will be used to verify the aerodynamic approach including conditions with sideslip.

**Figure 9: Already manufactured parts of the current LFBB wind tunnel model**

During the aerodynamic design and analysis, which is discussed more detailed in reference 11, several configurations without and with canard have been considered. The results indicate severe problems concerning longitudinal stability and trim for the early configuration without canard (Figure 10).

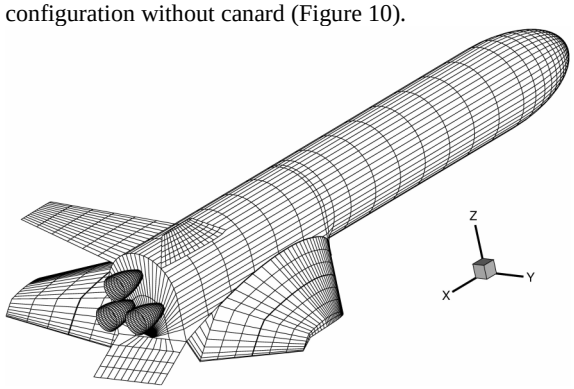


**Figure 10: Early LFBB configuration "Y6" without canard, $\eta_{bf}$=30°, $\eta_{wf}$=30°**

The trim of this vehicle is only possible for M < 5.6 and assuming an actually not achievable far backward position of the centre of gravity at $x_S/l$=0.75. The required flap deflections are even now in the order of η=30° in hypersonic flow and more than η = -10° for M < 2. Another disadvantage is the fact that this configuration is highly unstable. Based on these findings it has been decided to investigate LFBB configurations with canards.

The fuselage geometry has to remain unchanged due to the requirements of the acceleration mission.

During the Euler calculations and trim analysis for the most promising vehicle with canards (dubbed configuration "Y-7"), the small bodyflap is fixed at η=5°, the wing is clean and only the canards are deflected for trim (compare transonic flow conditions in Figure 11).

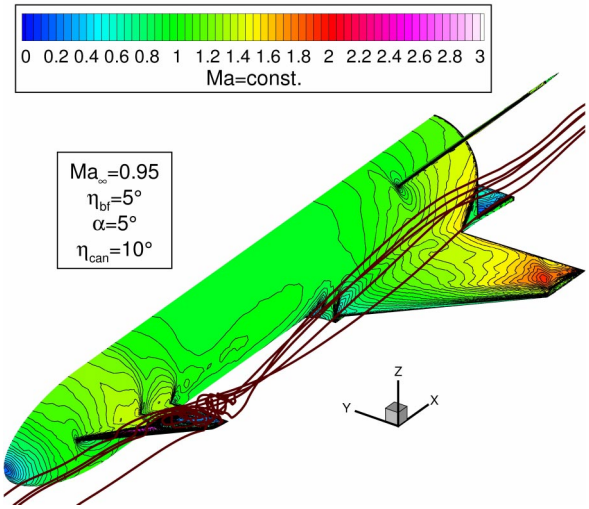


**Figure 11: Flowfield and Mach number contours on recent LFBB vehicle "Y-7" at M= 0.95 (Euler calculation)**

With view to the required canard deflection along the reentry and return flight trajectory (Figure 12) it is obvious that "Y7" is robust for the approximately actual position of the centre of gravity at 62 % of vehicle length ($x_S/l$=0.62).

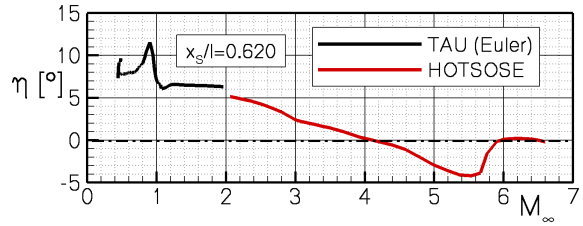


**Figure 12: Canard deflections for vehicle "Y7" along return flight trajectory**

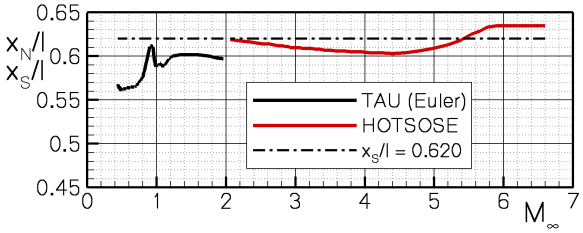


**Figure 13: Stability margin of vehicle "Y7" along return flight trajectory**

The obtained deflections are always smaller than η=5° for M > 2 and in the order of η=8° during the cruise flight at M=0.5. The configuration is stable for M > 5.5, but unfortunately a stability problem is detected at the cruise flight conditions of M=0.5 (Figure 13). A detailed aerodynamic analysis of the problem is given in ref. 11. Although active control (compare chapter 6.2) should not be completely ruled out, options to find an acceptable solution in this important flight regime will be analysed in the near future, regarding an updated vehicle cog and additional aerodynamic data. The analysis of the wind tunnel force measurements will allow a final analysis of subsonic cruise flight, and based on these results the wing is going to be adapted. The goal is to stabilise the vehicle, which allows to minimise the required canard deflections for trim during cruise conditions.

The second focus of the aerodynamic investigations is the assessment of the aerodynamic interactions between Ariane 5 core stage and the LFBB's during mated ascent. With view to the structural layout of wing and body performed (see chapter 5), especially the flight condition with maximum dynamic pressure at M=1.6 is of interest. Due to the fact that the configuration is asymmetric for lateral flow conditions the complete configuration has to be considered (Figure 14).

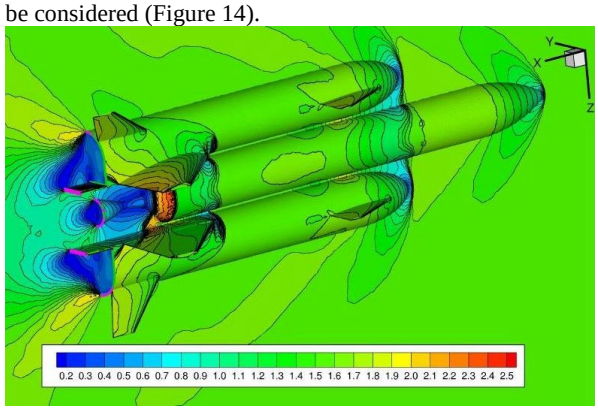


**Figure 14: Flowfield and Mach number contours around the Ariane 5 and two attached LFBB at M= 1.6, α=0°, $\eta_{can}$=0° (Euler calculation)**

In order to extract the aerodynamic interactions on the structural loads the isolated LFBB is compared to the combination of Ariane 5 with two LFBB without and including attachment structure between rocket and booster. As an engineering approach Euler calculations using an unstructured mesh are applied (see reference 11). The flowfields and the obtained structural loads are used as the basis for the mechanical layout of the vehicle.

## 5 MECHANICAL LAY-OUT OF VEHICLE STRUCTURE

In this phase of the ASTRA-study a preliminary mechanical design of major structural elements is performed. This work is executed by the German launcher industry Astrium and MAN. The wing, thrust frame, tanks, and fuselage are dimensioned according to the operational loads calculated from flight dynamic and aerodynamic analyses.

The main function of the booster structure is to transfer the thrust into the EPC-stage. The load introduction is foreseen at the forward attachment, in order to keep the same structural architecture as for the EPC of the present Ariane 5. The booster thrust is submitted from the thrust frame via the rear fuselage, through the LH2 and LOX tank to the attachment ring structure into the EPC.

### 5.1 Tank, Fuselage and Wing Structure

The general loads for dimensioning of the fuselage take into account:

- the axial loads during ascent caused by thrust, inertia loads and aerodynamic drag
- the axial flux distribution (warping forces) due to the booster load introduction
- bending moments during ascent due to lateral aerodynamic loads (an effective angle of attack due to wind and gusts of 5° at maximum dynamic pressure is assumed) and lateral dynamic loads, which are supposed to be quasi-static with ± 1 g
- bending moments during descent (the maximum bending moment occurs at M= 5.6 with an angle of attack of 16° and a dynamic pressure of 27300 Pa leading to 3.5 g lateral acceleration)

Axial loads of the descent flight phase are neglected. While for the fuselage the ascent flight is the dimensioning case, the descent flight gives the maximum load for the wing. All aerodynamic loads (in form of pressure distributions), coming from 3-D numerical analysis (see chapter 4) are transferred automatically to the 3-D structural code (finite element program NASTRAN).

At the LFBB's top the nose cap structure is attached, which is an aerodynamic cover and completely removable for easy accessibility in case of maintenance.

The load carrying LH2 and LOX tank as part of the forward fuselage as well as the attachment ring structure (see chapter 5.2), are designed similar to the Ariane 5 EPC tank and front skirt JAVE. The minimum and maximum internal pressures of the integral LOX and LH2 tank are taken from the Ariane 5 EPC tank.

The axial force fluxes (warping fluxes) due to booster load introduction depend on the design and wall stiffness of the attachment ring and the tank structure. Therefore, an iterative sizing approach is necessary. It turns out, that the warping fluxes due to the load introduction are still effective within the cylindrical part of the LOX tank, but "die out" with the beginning of the LH2 tank. Figure 15 shows the axial force flux distribution obtained from a finite element analysis.

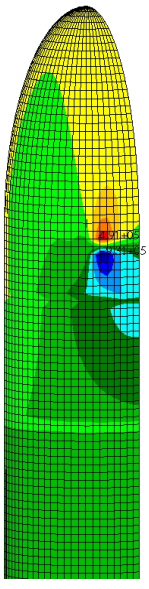

**Figure 15: Axial Force Flux due to Load Introduction from attached Core Stage**

The cylindrical tank parts are integrally stiffened with the stiffening outside. Since the insulation is foreseen externally, an internal inspection of the tank skin is possible.

The tank sizing is made for the two materials Al 2219 (as used in Ariane 5) and the aluminum lithium alloy Al 2195. A mass optimization has been performed (pocket size, skin thickness, stage thickness and height) regarding strength, global buckling, local buckling, and manufacturing constraints (minimum thickness, number of pockets). The isogrid stiffened type turns out to be the lightest design. The bare (non-equipped) integral tank mass is calculated to:

Al 2219 : 4580 kg
Al-2195 : 4040 kg

The sizing of the wing and the rear fuselage has also been done by an iterative approach. In a first step the important structural members are pre-designed and dimensioned with use of local FE-models, manual calculations, and estimated interface forces. As an example, Figure 16 shows a design sketch of a ring frame in the rear fuselage loaded by wing interface forces.

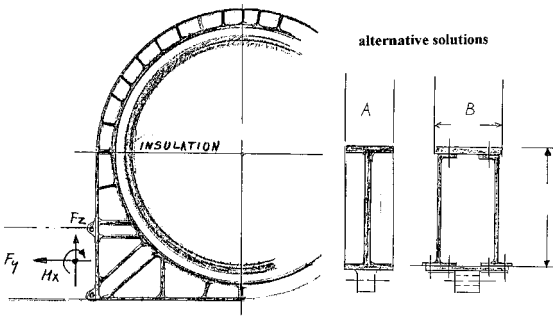


**Figure 16: Ring Frame Design for the Rear Fuselage**

The result of such a frame pre-dimensioning is shown in Figure 17 as a stress plot.

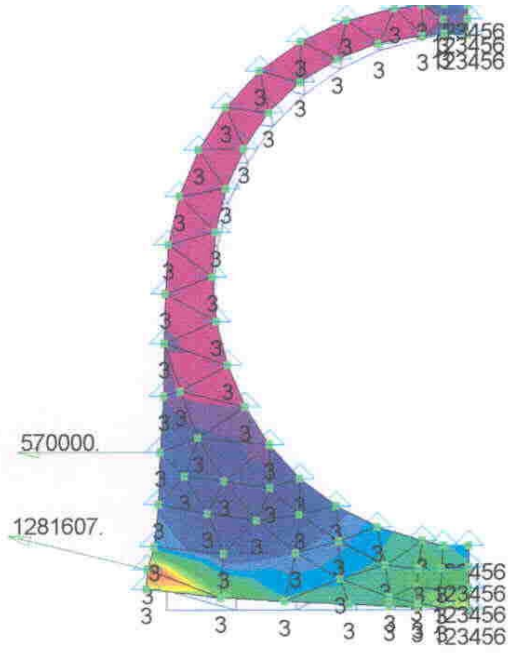


**Figure 17: Stress Plot of a Ring Frame at the Rear Fuselage**

Then a course 3-D finite element model based on the chosen structural concept is made, representing the stiffness of structural members. This model, called static system model (Figure 18), delivers the internal loads (force fluxes in ring frames, shear loads in panels) when the external loads are applied. Within parametric investigations the properties of the structural members are modified in order to reach minimum mass. Strength and stability analyses are done with more detailed finite element models.

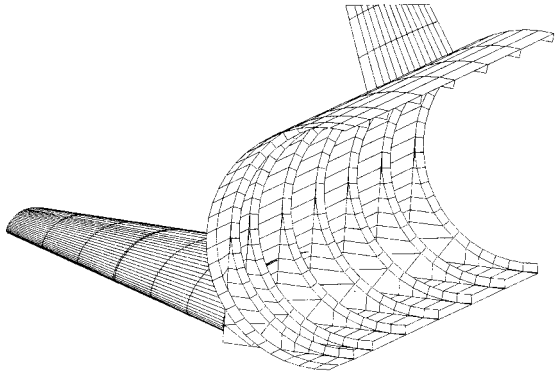

**Figure 18: Static System Model for Internal Loads**

The rear fuselage is proposed to be made of CFRP, locally reinforced against buckling.

The structural concept of the wing is shown in Figure 19. The wing box has four spars and it is stiffened with ribs. The shear panels are designed as CFRP sandwich panels, reinforced by T-sections at the lower and upper end.

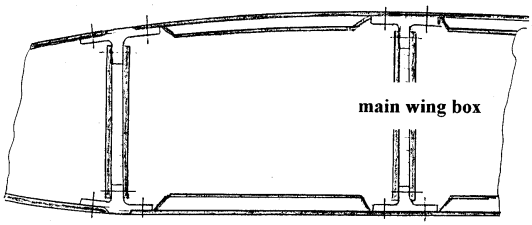


**Figure 19: Wing Box Structural Concept**

The finite element model for stress and buckling verification is shown in Figure 20 and a corresponding stress plot is given in Figure 21.

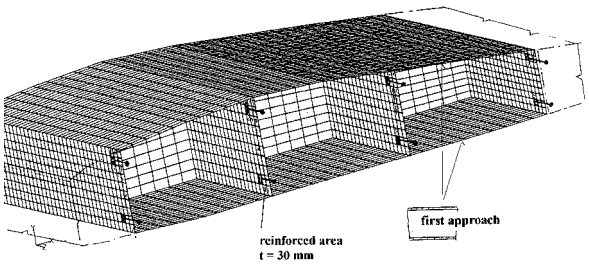


**Figure 20: FE-Mesh of the Wing Box**

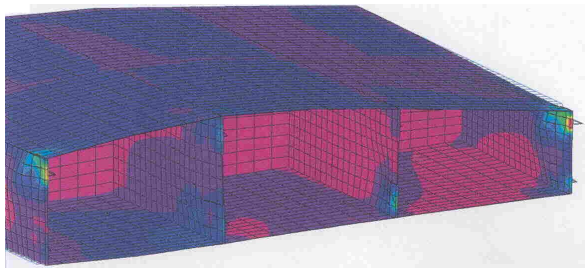

**Figure 21: Stress Plot of the Wing Box**

For the thrust frame a trade-off between a truss structure (CFRP struts) and a conical shell has been performed. It turns out that the shell structure, also made of CFRP, has more advantages. A stress plot of the selected thrust frame for the three Vulcain 3 engines is shown in Figure 22.

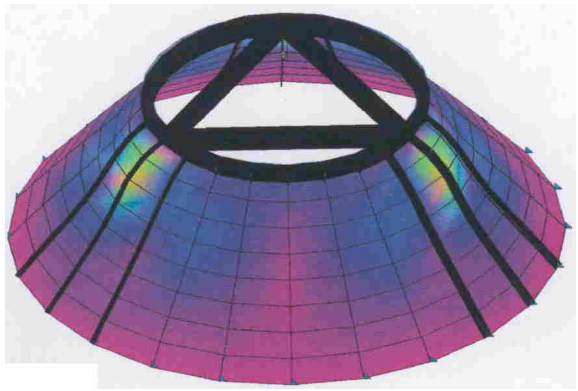

**Figure 22: Stress Plot of the Thrust Frame**

The overall structural mass (without thermal protection and equipment) of the rear fuselage, wings, fins, thrust frame and non-integral second LH2 tank has been determined by the structural analysis to arrive at about 10370 kg

Stiffness requirements, which can influence the structural mass, are not defined yet. They have to be derived from dynamic and aeroelastic investigations, which are foreseen in the next study phase.

## 5.2 Attachment Structure

To get a more detailed knowledge of the mechanical architecture an in depth analysis of the booster attachment ring is performed. Its basic design should be analogous to the Ariane 5 EPC forward skirt, but it is especially equipped to take care for the requirements of a reusable re-entry vehicle.

This ring is located between the forward end of the oxygen tank and the LFBB's nose section. It is one of the main structural elements of the booster with very high loads and several interfaces like the canard support and the main attachment fitting, introducing the thrust loads to the expendable core stage. The length of the ring is 2.5 m with the booster's external diameter of 5.45 m.

The main task of the attachment ring is to transfer the booster's thrust loads to the core stage. As with today's Ariane5 all axial thrust is transferred at the forward end of the booster into the front skirt JAVE above the EPC. The highest load on the main fitting is reached shortly before the LFBB's separation, and reaches a peak value of almost 3000 kN. The ring further transmits the loads from the air

breathing engines, from the nose landing gear and from the canards. It houses the mechanism of the canard actuation, the two forward separation rocket motors and other secondary structures.

The preliminary structural lay-out is shown in Figure 23. The basic design is similar to the Ariane 5 EPC forward skirt. But as the booster skirt is unsymmetrically loaded, it has a strong section around the attachment fitting and a considerably thinner and lighter region on the opposite side. The nose landing gear is located inside the nose assembly close to the ring structure. Therefore, it is possible to attach the gear's strut support to the same major frames of the ring, which already transfer the thrust loads during ascent. (see Figure 24) The multiple use of structural elements during different phases of the booster mission enables considerable weight savings.

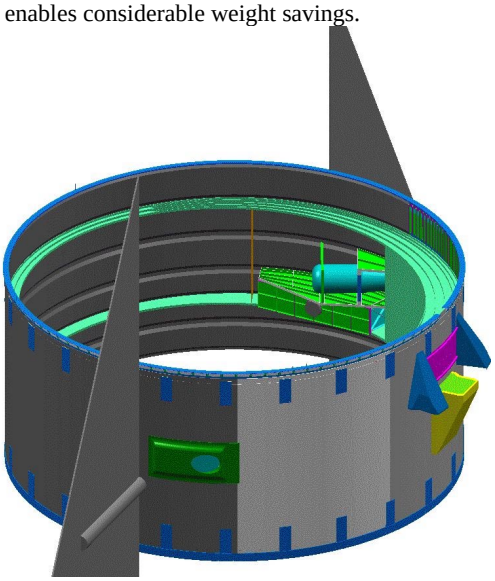

**Figure 23: Preliminary design of LFBB attachment ring showing the stage attachment on the right and the support structure for separation motors and canard actuation inside**

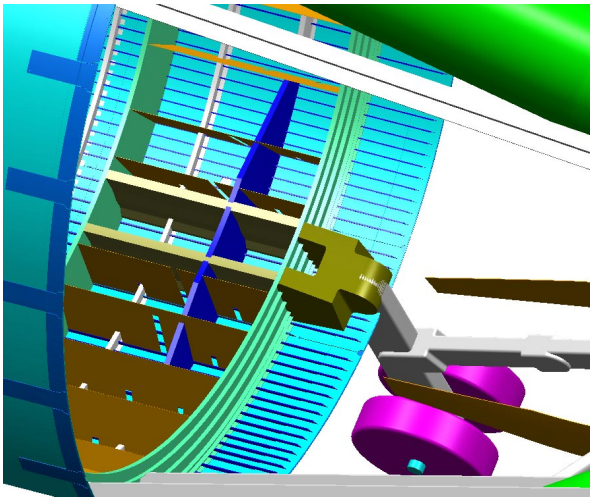

**Figure 24: Preliminary design of LFBB attachment ring showing the internal lay-out including the support structure of the nose landing gear**

The general layout of this ring comprises:

- a load carrying outer skin made of integrally stiffened Al-panels in the highly loaded area and CFRP sandwich panels in the lightly loaded area opposite the main fitting
- two major frames to accommodate the radial loads
- an inner skin building a closed box with the outer skin and the frames that takes up the torsion and bending loads from the main fitting.

Because of the booster's reusability all parts have to be designed to ease inspection and to allow replacement of damaged parts with little effort. Especially limited lifetime parts (e.g. separation motors) have to be considered carefully in their accessibility.

During the re-entry flight the booster is subject to increased aero-thermal heating. To protect the outer skin against this heat flow a thermal protection has to be used. Preliminary estimation of the heat flux indicates that on the windward side a flexible insulation like AFRSI would be sufficient.

For the analysis and iterative design optimization of the structure a finite element model has been built. This model consists of 7000 elements, six load cases are calculated and the computing time is approximately 2 minutes each. Due to this quick tool it is possible to perform basic optimizations very easily. Figure 25 shows the FEM-structure. Adjacent structural items (e.g. the LOX-tank) are also modeled to get realistic boundary conditions.

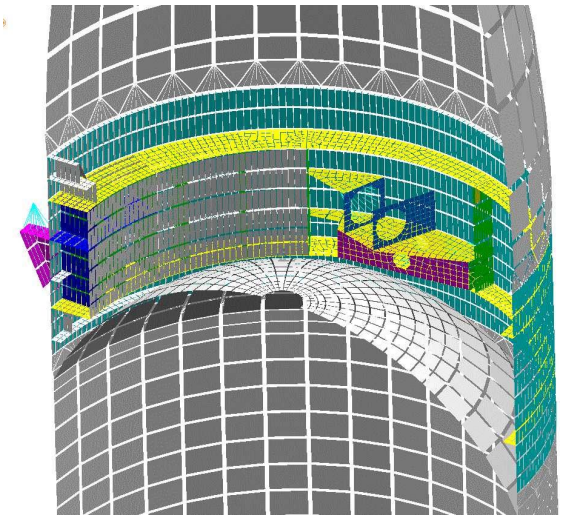

**Figure 25: FEM half model of the attachment ring structure**

Based on this FE-model the mass of the ring structure is calculated. For all single parts the material thickness is taken from the optimized finite element model and the parts are designed in the CATIA-3D CAD-tool to include the mass of flanges and stringers.

The mass of the complete attachment ring structure, derived from this preliminary but detailed structural investigation is found at 691 kg.

## 6 SYSTEM PERFORMANCE

### 6.1 Ascent flight optimization

The usual mission of commercial Ariane 5 flights will continue to be operated from Kourou to a 180 km x 35786 km GTO with an inclination of 7 degrees. This orbit data and a double satellite launch including the multiple launch

structure SPELTRA are assumed. The overall ascent trajectory of Ariane 5 with LFBB is similar to the generic GTO flight path of Ariane 5 with SRM. After vertical lift-off the vehicle turns during a pitch maneuver, and heads eastward to its low inclined transfer orbit. This trajectory has to respect certain constraints, which are close to those of Ariane 5+ ascent. Throttling of the Liquid Fly-back Booster is not performed, since the Ariane 5 acceleration limit is not reached.

Some characteristic mass data of the investigated LFBB configuration as of August 2002 is listed in Table 3. The dry mass is already partially incorporating the results of the structural analyses of chapter 5. The separated satellite payload mass in double launch configuration exceeds 13 Mg. The fully cryogenic launcher (boosters, core, and upper stage) is able to deliver almost 2 % of its gross lift-off mass into GTO.

| | kg |
|---|---|
| **LFBB dry mass:** | **47500** |
| **GLOW LFBB mass:** | **220500** |
| **GLOW launcher mass:** | **695775** |
| **GTO payload mass:** | **13250** |

**Table 3: Characteristic mass data of the Fly-back Booster for GTO mission with Ariane 5 core stage**

## 6.2 Descent and Return Flight

Initial re-entry and return flight mass of each LFBB is 54460 kg, which is below the MECO-value, because the aft part of the stage attachment is jettisoned, and the solid propellant of the separation motors is already burned. During the ballistic phase of the trajectory the remaining oxygen in the tank and in the fuel lines will be drained.

Aerodynamic data sets of the booster's return flight configuration have been generated in the aerodynamic analysis of chapter 4. Lift-, drag-, and pitching moment coefficients with regard to canard and bodyflap deflection are used in combination with a calculation of center of gravity movement, to perform a flight dynamics and control simulation. The trimmed hypersonic maximum lift-to-drag ratio reaches about 2.0. In the low subsonic and cruise flight regime trimmed L/D is slightly above 5.0. Hypersonic trimming is performed by the canards and supported by the RCS. A stable condition is achievable at least up to angles of attack of 35 degrees. For this type of LFBB 35 deg. are used as the upper limit during return flight.

Due to the remaining flight path angle of about 25 degrees at staging the LFBB climbs in a ballistic trajectory above 90 km. Falling back the booster still reaches a velocity close to the separation conditions of 1.95 km/s (about Mach 6) at 50 km, since the atmospheric drag is low. Although the angle of attack is held at the 35 deg. limit, a steep trajectory is performed due to the restricted dynamic pressure and lift force, with a path angle $\gamma$ diving as low as -23°.

When entering the denser layers of the atmosphere the aerodynamic forces rapidly increase, finally stabilizing the LFBB altitude, and achieving maximum deceleration at an altitude of around 20 km. The simulation is performed under a closed control loop, which regulates the trajectory within normal load boundaries, as far as flap efficiency is available. An optimal trajectory is found by parametric variation of the initial banking maneuver. The return of the LFBB should start as early as possible, but is not allowed to violate any restrictions. The banking is automatically controlled to a flight direction with minimum distance to the launch site. After turning the vehicle, the gliding flight is continued to an altitude of optimum cruise condition.

An elaborate method is implemented to calculate the required fuel mass of the turbojets for the powered return flight to the launch site. The complete flight is controlled along an optimized flight profile. Aerodynamic data, vehicle mass, and engine performance (available thrust and sfc) are analyzed in such a way, to determine the stable cruise condition with the lowest possible fuel consumption per range (g/km). This is not a trivial task, since engine performance is dependent of altitude and Mach number, and the equivalence of drag-thrust respectively lift-weight is usually not exactly found at maximum L/D. The changing booster mass due to fuel consuming, and a minimum necessary acceleration performance have also to be taken into account.

The powered return trajectory is automatically controlled to follow the optimum flight condition, always directly heading to the launch site. Fuel flow is integrated to get its exact amount. In case of the most recent LFBB configuration, a specific complication has to be addressed. As the aerodynamic calculations show, the vehicle seems to be subject to an unstable condition during cruise flight. Even though, future improvements of the aerodynamic shape should avoid this difficulty, the flight dynamics simulation demonstrates that under realistic canard actuator conditions the LFBB is fully controllable by active means. The main parameters for vehicle control are depicted in Figure 26 along return flight. Note that the shown Mach number dependency of the canard deflection is similar but not identical to that in Figure 12 due to the flight dynamics simulation performed here with regard to cog movement.

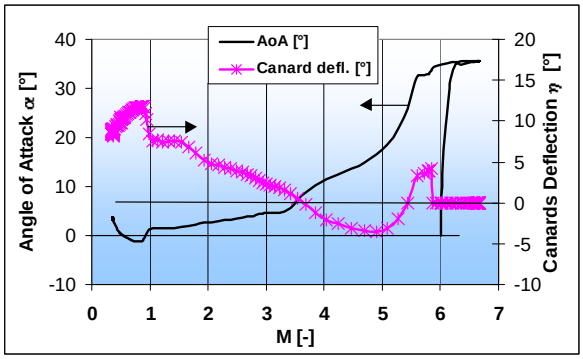


**Figure 26: Control parameters $\alpha$ and $\eta_{Canard}$ of the LFBB re-entry and return flight trajectory from flight dynamics simulation**

Including 20% fly-back fuel reserves to take into account adverse conditions like head winds, the booster needs about 4.1 Mg hydrogen for its more than one hour return leg.

## 7 CONCLUSION

Technical investigations on a partially reusable space transportation system with reusable booster stages, attached to an advanced future derivative of the expendable Ariane 5 core stage, demonstrate the feasibility of several promising design features. The fully cryogenic launcher is able to deliver more than 13000 kg of payload into GTO.

The reusable boosters are designed with the same external diameter as Ariane5's EPC, the large integral tank is of similar architecture, and the basic lay-out of Ariane 5's forward skirt JAVE is reused for the LFBB's attachment ring. Therefore, existing manufacturing infrastructure might be continuously operated for the RLV assembly. The wing and fuselage structure also incorporates advanced materials like CFRP.

An aerodynamic vehicle configuration with two large canards, a clean wing, and an aft-positioned bodyflap is selected. Numerically calculated aerodynamic data sets for the complete trajectory (M= 0.27 up to M= 7.0) have been prepared. Canard deflections for trimming remain within a moderate range. However, in the subsonic fly-back cruise regime a vehicle stability problem is detected. Wind tunnel tests of the LFBB scheduled for the near future, will support an adaptation of the wing to eventually reach a naturally stable configuration.

Flight dynamics simulations of the launcher with winged stages subject to atmospheric perturbations have been performed. It can be proofed that the controllability of the examined configuration during the mated ascent until separation is achievable, if all booster engines are available for two dimensional thrust vector control. The study indicates that the ascent flight requirements of control seem to be *not* the dimensioning factor for wing layout and positioning. A return trajectory flight simulation demonstrates that under realistic canard actuator conditions the LFBB is fully controllable by active means despite its stability problem.

Future work on the described Liquid Fly-Back Booster will address a further enhancement in system robustness and cost efficiency. Besides the already mentioned aerodynamic improvement, dynamic and aeroelastic investigations of the structure are foreseen. Selection of major subsystems, fly-back turbojet integration issues, as well as vehicle health monitoring will be covered.

All applied technologies of the LFBB-RLV are well within reach for Europe in the next 10 years. When satisfactory operational efficiency is achievable, reusable booster stages represent an interesting and serious option in the future European launcher architecture.

## 8 REFERENCES


1. Sippel, M.; Herbertz, A.; Kauffmann, J.; Schmid, V.: Investigations on Liquid Fly-Back Boosters Based on Existing Rocket Engines, IAF 99-V.3.06, 1999

2. Sippel, M.; Atanassov, U.; Klevanski, J.; Schmid, V.: First Stage Design Variations of Partially Reusable Launch Vehicles, J. Spacecraft, V.39, No.4, pp. 571-579, July-August 2002

3. Klevanski, I.; Herbertz, A.; Kauffmann, J.; Schmid, V. Sippel, M.: Aspekte der Stabilität und Steuerbarkeit in der Flug- und Separationsphase unsymmetrischer Trägerkonfigurationen, DGLR-JT2000-165, 2000

4. Sippel, M.: Programmsystem zur Vorauslegung von luftatmenden Antrieben für Raumtransportsysteme, abp 2.0, DLR TB-319-98/07, 1998

5. Edwards, P.R.; Svenson, F.C.; Chandler, F.O.: The Development and Testing of the Space Shuttle Reaction Control Subsystem, ASME-paper 78-WA/AERO-20, 1978

6. Seidel, A.; Pulkert, G.; Wolf, D.: Development History of Small $H_2/O_2$- and $H_2/F_2$-Engines for Advanced AOCS-, RVD- and OMS-Systems, AIAA Paper 91-3389, 1991

7. Klevanski, J; Sippel, M. : Beschreibung des Programms zur aerodynamischen Voranalyse CAC Version 1.0, SART TN-003/2001, DLR-IB 645-2001/02, 2001

8. Klevanski, J.; Burkhardt, H.; Sippel, M.: Parametrical Analyses of Liquid Fly Back Booster Ascent Controllability, ASTRA Doc. No. 1000-008, SART TN 001/2002, DLR-IB 645-2002 / 02, 2002

9. Mack, A; Hannemann, V.: Validation of the Unstructured DLR-TAU-Code for Hypersonic Flows, AIAA Paper 2002-3111, 2002

10. Reisch, U.; Anseaume, Y.: Validation of the Approximate Calculation Procedure HOTSOSE for Aerodynamic and Thermal Loads in Hypersonic Flow with Existing Experimental and Numerical Results, DLR-FB 98-23, 1998

11. Eggers, Th.; Božić, O.: Aerodynamic Design and Analysis of an Ariane 5 Liquid Fly-Back Booster, AIAA Paper 2002-5197, 2002


*Further updated information concerning the SART space transportation concepts is available at:*
http://www.dlr.de/SART